Parker Solar Probe observations of solar wind energetic proton beams produced by magnetic reconnection in the near-Sun heliospheric current sheet

T. D. Phan[1], J. L. Verniero[2], D. Larson[1], B. Lavraud[3,4], J. P. Eastwood[5], M. Øieroset[1], J. F. Drake[6], S. D. Bale[1,7], R. Livi[1], J. S. Halekas[8], P. L. Whittlesey[1], A. Rahmati[1], M. Pulupa[1], R. J. MacDowall[2], P. A. Szabo[2], A. Koval[2], M. Desai[9], S. A. Fuselier[9], M. Velli[10], M. Hesse[11], P. S. Pyakurel[1], K. Maheshwari[1], J. C. Kasper[12], J. M. Stevens[13], A. W. Case[13], and N. E. Raouafi[14]

[1] SSL, University of California, Berkeley, CA 94720, USA; phan@ssl.berkeley.edu

[2]NASA Goddard Space Flight Center, Greenbelt, MD, USA

[3]Laboratoire d'Astrophysique de Bordeaux, Univ. Bordeaux, France

[4]IRAP, CNRS, CNES, Université de Toulouse, France

[5]The Blackett Laboratory, Imperial College London, London, UK

[6]University of Maryland, College Park, MD, USA

[7]Physics Department, University of California, Berkeley, CA 94720-7300, USA

[8]University of Iowa, Iowa City, IA 52242, USA

[9]Southwest Research Institute, San Antonio TX, USA

[10]University of California, Los Angeles, Los Angeles, CA, US

[11]NASA Ames Research Center, Mountain View, CA, USA

[12]Climate and Space Sciences and Engineering, University of Michigan, Ann Arbor, MI, USA

[13]Smithsonian Astrophysical Observatory, Cambridge, MA, USA

[14]Johns Hopkins University Applied Physics Laboratory, Laurel, MD, USA

Abstract

We report observations of reconnection exhausts and associated ion and electron separatrix layers in and around the Heliospheric Current Sheet (HCS) during PSP Encounters 08 and 07, at 16 R_s and 20 R_s. HCS reconnection accelerated protons to almost twice the solar wind speed and increased the proton core energy by a factor of ~3, due to the Alfvén speed being comparable to the solar wind flow speed at these near-Sun distances. During E08, accelerated protons were found to have leaked out of the exhaust along separatrix field lines, appearing as field-aligned energetic proton beams in a broad region outside the HCS. Concurrent dropouts of strahl electrons, indicating disconnection from the Sun, provide further evidence for the HCS being the source of the beams. Around the HCS in E07, there were also proton beams but without electron strahl dropouts, indicating that their origin was non-local and closer to the Sun.

Plain Language summary

Magnetic reconnection in current sheets is a universal plasma process that converts magnetic energy into particle energy. The process is important in many laboratory, solar, and astrophysical plasmas. The heliospheric current sheet (HCS), which originates from the Sun and extends throughout the heliosphere, is the largest current sheet in the solar system. One of the surprises of the Parker Solar Probe mission is the finding that magnetic reconnection is almost always active in the near-Sun HCS, despite its enormous scales. In this paper, we report direct evidence showing that reconnection in the HCS close to the Sun can be a source of energetic protons observed in the solar wind. The reason protons can be accelerated to high energies (to tens of kilo-electronvolts) is because the available magnetic energy per particle is high close to the Sun. This finding is important because it is a mystery where energetic protons in the heliosphere come from.

Key points:

- Large available magnetic energy led to significant proton acceleration by reconnection in the near-Sun HCS detected at 16 R_s and 20 R_s.
- Leaked exhaust protons and strahl electron dropouts in separatrices provide evidence for HCS source of proton beams in the solar wind.
- Energetic protons beams outside the HCS also exist without strahl electron dropouts. Their origin is likely non local and closer to the Sun.

1. Introduction

Magnetic reconnection converts magnetic energy into particle energies. In the solar wind at 1 AU, reconnection exhausts have been detected in Interplanetary Coronal Mass Ejections (ICME), in random solar wind current sheets, and occasionally in the HCS (e.g., Gosling et al., 2005a,b; 2006; Phan et al., 2006; Davis et al., 2006; Huttunen et al., 2008; Eriksson et al. 2009, Ruffenach et al. 2012; Lavraud et al. 2009; 2014; Mistry et al. 2015; 2017).

The most commonly reported in-situ signatures of reconnection in solar wind current sheets are fluid signatures such as Alfvénic plasma jetting and heating (e.g., Gosling et al., 2005a; Phan et al., 2006; Drake et al., 2009; Pulupa et al., 2014). Kinetic signatures of reconnection such as counterstreaming ions have also been seen inside some solar wind exhausts (Gosling et al., 2005a; Lavraud et al., 2021), as have electron signatures of the separatrix layers bounding the exhaust (Gosling et al., 2005a;b; 2006; Lavraud et al., 2009; Phan et al., 2021). Ion separatrix signatures in the form of proton beams have also been reported by Wind (Huttunen et al., 2008), and recently by Solar Orbiter at a reconnecting current sheet associated with a magnetic switchback (Lavraud et al., 2021).

In the solar wind at 1 AU, the available magnetic energy per particle, $m_iV_A^2$ (Phan et al., 2013), is only ~25 eV (for a typical V_A~ 50 km/s), where m_i is proton mass and V_A the Alfvén speed. Thus, the energy increase associated with reconnection plasma jetting and heating is small compared to the core solar wind flow energy of ~1 keV. Furthermore, the high plasma β environment at 1 AU is less favorable for reconnection to be triggered in the local solar wind current sheets (Swisdak et al., 2003; 2010; Phan et al., 2010). Indeed, reconnection is detected in only a small fraction of solar wind current sheets at these distances, and it is therefore not energetically important in terms of the evolution of heliospheric plasmas and fields (Gosling, 2007). Nevertheless, energetic ions up to MeV energies have been seen near some reconnecting current sheets at 1 AU (e.g., Khabarova et al., 2015; 2017). The open question is whether they originate from the local current sheet or at a site closer to the Sun, and whether they are associated with reconnection or other processes.

Parker Solar Probe (PSP) provides a unique opportunity to examine this question, since as its perihelion lowers, it samples the solar wind with increasing magnetic energy per particle, because of the higher Alfvén speed that is found in the near-Sun solar wind. During the first several orbits, PSP detected reconnection exhausts in current sheets associated with the HCS, ICMEs, magnetic flux ropes (Phan et al., 2020; Szabo et al., 2020; Lavraud et al., 2020), and at the boundaries of some magnetic 'switchbacks' (Froment et al., 2021). However, the great majority of small-scale and intense current sheets associated with 'switchbacks' did not show reconnection signatures (Phan et al., 2020; Akhavan-Tafti et al., 2021). Suprisingly, reconnection was commonly detected in the large-scale HCS, despite the local HCS thickness observed by PSP typically being thousands of ion inertial lengths (Phan et al., 2021).

In this paper, we report PSP observations of reconnection exhausts with ion and electron separatrix signatures during Encounters 08 and 07 (hereafter referred to as E08 and E07) crossings of the HCS. These events occurred close to perihelia, at 16 R_s and 20 R_s. The main finding reported here is that near-Sun HCS reconnection can produce energetic proton beams seen in a broad region outside the HCS.

The paper is organized as follows. Section 2 describes the data used in this study. We first describe the E08 HCS in Section 3, which helps contrast and understand the E07 HCS described in Section 4. We discuss open questions in Section 5.

2. Data and coordinate system

We use 4 samples/s magnetic field data from the FIELDS fluxgate magnetometer (Bale et al., 2016) and 0.87s-resolution proton data from the SWEAP/SPAN-ion instrument (Livi et al., 2020). We also use core electron temperature moments (Halekas et al. 2020) and pitch angle information of 314eV electrons measured by the SWEAP/SPAN-electron instrument (Kasper et al., 2016; Whittlesey et al., 2020), and energetic ion data obtained from double coincidence time-of-flight measurements by the ISOIS/EPI-Lo instrument (McComas et al., 2016).

For simplicity we display all data in RTN coordinates because the E07 and E08 HCS lay extremely close to the **R**-**T** plane (see the Supporting Information section). However, for the determination of the HCS thickness, we use the measured normal velocity in the spacecraft frame and in the current sheet coordinate system.

3. E08 HCS

We describe E08 before E07 because the HCS origin of the proton beams is much clearer in E08. The understanding of E08 raises questions about the source of proton beams seen in E07.

3.1. Overview

Figure 1 shows the PSP crossing of the HCS on 2021 April 29, at 08:14:23-08:28:16 UT (between the two black vertical dashed lines at 't_1' and 't_2'). The HCS crossing is recognized by the polarity change of B_R (Figure 1f) and switching of strahl electron pitch angle fluxes from 0° to 180° (Figure 1d) across the current sheet. The crossing occurred at perihelion, ~16 R_S from the Sun. The magnetic field strength was ~400 nT before the HCS crossing, and ~330 nT after. From 08:28:16 UT ('t_2') to 08:51:30 UT ('t_3'), PSP seemed to linger near the exhaust boundary while dipping occasionally back into the exhaust as suggested by several strahl dropouts (panel d) and radial velocity increases (panel g). Finally it reached the solar wind proper at 't3', where |**B**| reached close to its pre-HCS value of 400 nT. Thus, there are some uncertainties about the true location of the trailing edge of the HCS.

The magnetic field rotation across the current sheet was 162°, i.e., the guide field was small. The HCS was bifurcated, with sharp changes in B_R at the two edges (Figure 1f). The solar wind proton density was ~2400 cm^{-3} prior to the HCS, and ~4400 cm^{-3} after. The hybrid Alfvén speed based on B_R and the proton mass density ρ on the two sides of the HCS, $V_{AR,hybrid}$= $[B_{R1}B_{R2}(B_{R1}+B_{R2})/\mu_0(\rho_1 B_{R2}+\rho_2 B_{R1})]^{0.5}$ (Cassak and Shay, 2007), was ~134 km/s. The proton and electron β were 0.15 and 0.32 prior to and 0.40 and 0.86 after the HCS crossing.

The duration of the HCS crossing (between 't_1' and 't_2') was ~833 seconds, which translates to an exhaust width (along the current sheet normal) of 1.8×10^4 km, or ~4620 ion inertial lengths

(d_i), based on the measured normal velocity of the current sheet relative to the spacecraft of ~21 km/s (not shown).

3.2. Proton bulk acceleration and bulk heating

Figure 1g shows that inside the current sheet there was a proton radial flow acceleration ΔV_R ~140 km/s (relative to the external solar wind V_R of ~210 km/s), with opposite δV_R-δB_R correlations upon entry and exit of the bifurcated HCS, consistent with reconnection (Gosling et al., 2005a). The jet speed was close to the hybrid Alfvén speed of 134 km/s, in close agreement with reconnection predictions (Cassak and Shay, 2007). The positive ΔV_R jet implies an anti-sunward directed exhaust, i.e., the X-line was located sunward of PSP (Figure 1k).

Also consistent with reconnection are density (Figure 1h) and proton temperature (Figure 1i) enhancements inside the exhaust. The ~40 eV proton bulk heating in this event is substantially higher than the 1-2 eV heating seen in previous HCS exhausts observed by PSP further (>29 R_s) away from the Sun (Phan et al., 2021). The larger heating is roughly consistent with the expectation from the scaling of reconnection proton heating with the available magnetic energy per particle, $\Delta T_i \propto m_i V_A^2$ (Drake et al., 2009; Phan et al., 2014; Haggerty et al., 2015). On the other hand, there was no evidence for electron heating across the exhaust boundaries (Figure 1j).

3.3. Ion and electron separatrix signatures: Proton beams and strahl electron dropouts

As the solar wind protons were bulk accelerated by reconnection to 1.7 times the ambient solar wind speed (from 210 km/s to 350 km/s), Figure 1b shows that the solar wind proton core energy nearly tripled (from ~320 eV outside the HCS to ~900 eV inside). The tail of the proton spectra extended to at least 2.5 keV (Figure 1b), and data from the ISOIS/EPI-Lo instrument suggests the presence of ion intensity enhancements up to ~40 keV/nucleon in the exhaust and in the surrounding regions (Figure 1a). The energized proton population inside the exhaust is easily distinguishable from the ambient solar wind, which makes it possible to unambiguously identify proton beams that leaked out of the HCS, as we now describe.

Immediately outside and prior to the HCS, marked by the blue bar at the top of Figure 1, in a region where the magnetic field B_L was already at its asymptotic value of ~400 nT, there was a proton population at higher energies (extending to at least 2.5 keV) than the core solar wind. Figure 1a shows that the energy of this population extends to ~40 keV/nuc. The following observational evidence points to the source being reconnection-energized protons that leaked out of the HCS:

1. The high-energy population had a similar upper energy spectrum profile as the reconnection-accelerated proton population seen inside the HCS (Figures 1b, 2e-g).
2. There was an energy-dispersion of the low-energy cutoff of the high-energy population, with higher low-energy cutoff further away from the HCS (Figure 1b). The energy dispersion is consistent with velocity filter effects (e.g., Onsager et al., 1991; Lavraud et al., 2002): Leaked protons on separatrix field lines further from the current sheet had longer distances to travel, and could reach PSP only if they had sufficiently high energies. On separatrix field lines closer to the current sheet, protons with a broader range of energy could reach PSP, as observed.
3. The presence of proton beams coincided with strahl electron dropouts (Figure 1d), consistent with the separatrix field lines being disconnected from the Sun and connected to an exhaust anti-sunward of the X-line.

Further to the left of the HCS, there were intermittent detections of proton beams, also with concurrent strahl electron dropouts. We interpret these as partial PSP re-entries into the separatrix layer.

We now examine the proton distributions in and around the HCS. Figure 2g shows an example of a proton velocity distribution function (VDF) inside the HCS close to the left edge. The VDF was much broader than the core solar wind seen outside the current sheet (e.g., Figure 2e), and consisted (in the solar wind frame) of two field-aligned counterstreaming proton populations, providing evidence for magnetic connection across the exhaust (e.g., Gosling et al., 2005a; Phan et al., 2007; Eastwood et al., 2018; Lavraud et al., 2021). The VDF of the core population became more isotropic in the weak field region of the exhaust (Figure 2h). Outside the HCS, the VDF (in Panels e and f) consisted of a narrow (cold) core population and a higher energy anti-sunward (positive V_R) field-aligned component corresponding to protons that have leaked out of the HCS. Further from the HCS the leaked population consists of only the highest energies and looks 'detached' for the core (Panel e), while closer to the HCS (Panel f), a larger range of energies is seen, consistent with the velocity filter effect.

While the ion and electron separatrix signatures were clear on the side prior to the HCS, they were less clear after the HCS, partly because of the uncertainly about the location of the trailing edge of the HCS. If the trailing edge was at 't_2' (Figure 1), the absence of proton beams (Figure 1b) and 314 eV electron dropouts (Figure 1d) would imply a lack of a separatrix layer after the HCS, a result that is not consistent with traditional models of reconnection exhausts. If the trailing edge was at 't_3', there were proton beams to the right of the boundary. There were the expected simultaneous dropouts of strahl electron immediately after 't_3', but no strahl dropouts in much of the region with proton beams after that.

4. E07 HCS

4.1. Overview

Figure 3 shows a complete crossing of the HCS during E07 at 20 R_S (between the two vertical dashed lines). The HCS is characterized by a B_R reversal (Figure 3e) and concurrent switching of 314 eV electrons pitch angle fluxes from being predominantly field-aligned (0°) to anti-field-aligned (180°) (Figure 3c). The total field rotation across the HCS was 170°. Similar to the E08 HCS (Figure 1), there were modest magnetic field and density asymmetries across the HCS: |**B**| was 15% weaker (Figure 3d) and N_p was 1.5 times higher (Figure 3g) after the crossing. The proton and electron β were 0.25 and 0.53 before and 0.44 and 0.83 after the HCS.

The HCS crossing duration was ~1020s. With a measured current sheet normal velocity relative to the spacecraft of ~39 km/s, the current sheet width was ~4×10^4 km, or ~8530 d_i.

4.2. Proton bulk acceleration and heating

Proton V_R jetting was observed inside the HCS (Figure 3f). The jet speed was remarkably steady throughout most of the HCS, indicating laminar outflow. V_R was more variable in the last 3 minutes before the exit of the HCS where there were multiple bipolar variations of B_N which could indicate the presence of magnetic flux ropes (e.g., Eastwood et al., 2021). The V_R jet speed (relative to the adjacent solar wind flow) was ~ +125 km/s, close to the hybrid Alfvén speed of 120 km/s based on B_R~280 nT and N_p ~1720 cm^{-3} prior to HCS, and B_R~ -240 nT and N_p~2550 cm^{-3} after. The Alfvénic jetting is consistent with reconnection. The anti-sunward jet indicates an X-line located sunward of PSP.

There was also density compression (Figure 3g) and a ~30 eV proton temperature increase (Figure 3h) inside the exhaust, consistent with reconnection expectations. However, the core electron temperature decreased entering the exhaust from both sides (Figure 3i). This decrease is confirmed by a shift to lower energy of the peak in electron differential energy fluxes, as shown by the green curve in Figure 3b. The reduction in electron temperature in the exhaust is not an expected signature of reconnection (Phan et al., 2013; Pulupa et al.,2014).

4.3. Proton beams outside the HCS and the lack of strahl electron dropouts

The enhanced proton flow speed and heating inside the exhaust resulted in a shift to higher energies of the core protons by about a factor of three compared to the core solar wind outside the current sheet (Figure 3a).

Prior to the HCS crossing, there were bursts of anti-sunward and field-aligned energetic proton beams (Figure 3a), resulting in $T_{p||}$ enhancements (Figure 3h). Modest decreases in |**B**| and B_L during the proton beams were likely not associated with partial entries into the reconnection exhaust since the core solar wind population was not significantly accelerated (Figure 3a). Slight drops in the fluxes of the 314 eV field-aligned strahl electrons were observed in conjunction with these proton beams (Figure 3c), suggesting partial entries into the separatrix layer. However, the strahl electron dropouts were not significant compared to those discussed for the E08 separatrix layers in Section 3.3.

On both side of the HCS the 314 eV electrons were present all the way to the edge of the current sheet (marked by the dashed lines). In the region immediately outside the HCS on both sides, the proton spectra look like a core distribution with a suprathermal proton tail (Figure 3a). However, inspection of the VDFs in this region (not shown) reveals the presence of anti-sunward field-aligned beams, albeit at low fluxes. The upper energy of the low-flux beams is higher than the exhaust population, suggesting that they did not leak out of the local exhaust. The lack of leaked proton beams, coupled with no strahl dropouts, indicate the absence of separatrix layers outside the exhaust, which is not consistent with conventional reconnection models.

Zooming out, Figure 4 shows a broad region around the full and partial crossings of the HCS. Energetic proton beams (panel a) and associated temperature anisotropy $T_{p\|}$>>$T_{p\perp}$ (Figure 4h) were present over a very broad region surrounding the HCS, extending all the way to the two blue dashed lines ('t_1' and 't_6') in Figure 4. The ISOIS/EPI-Lo instrument detected ion intensity enhancements up to ~50 keV/nucleon throughout this broad proton beam regions (Desai et al., 2021). The appearance of proton beams in the vicinity of the HCS suggests that they are associated with the HCS. However, in contrast to E08, there were essentially no dropouts of 314eV electrons when the proton beams were observed. If these 314 eV electrons were strahl electrons from the Sun, their presence would mean connection to the Sun. This would be inconsistent with the region being magnetically connected to an anti-sunward HCS reconnection exhaust.

There may, however, be a different interpretation of the origin of the 314 eV electrons close to the E07 HCS. Figure 4b shows that there was an abrupt increase in the upper electron energy and a sudden broadening of the 314 eV electron pitch angle (Figure 4c) at 't_1' and 't_6', which mark where the temperature became persistently anisotropic $T_{p\|}$>>$T_{p\perp}$ (Figure 4h) due to the presence of proton beams. This suggests that the broader pitch-angle electrons adjacent to the HCS came from a different source than the narrower pitch-angle distributed electrons seen further away. It is likely that the narrower pitch-angle electrons are the usual strahls from the solar corona. The broader pitch-angle electrons, which have higher energies, could be from a different source. The concurrent presence of the proton beams and the broad pitch-angle electrons suggests is that they both originated from a common source sunward of PSP. The source is not likely to be the local HCS because the fluxes of 314eV electrons inside the local HCS were much lower than outside. On the other hand, it is unclear how electrons and protons from a remote source closer to the Sun, where energization (from reconnection or from another drive mechanism) might be stronger because of the higher available magnetic energy there, could penetrate to the region adjacent to the reconnection exhaust. For example, the separatrix field lines that bound the exhaust should divert particles produced by reconnection at a remote site away from the exhaust, just as strahl electrons are diverted.

5. Summary and Discussion

During Encounters 07 and 08, PSP encountered the HCS right around perihelia. Similar to previous PSP encounters where reconnection exhausts were detected at almost every complete HCS crossing (Phan et al., 2021), the E07 and E08 HCS displayed classic signatures of reconnection exhausts with Alfvénic outflows bounded by sharp slow-shock-like exhaust edges, across which the magnetic field magnitude dropped and the proton density and temperature increased (Petschek, 1964). At 16 R_s (E08) and 20 R_s (E07), the Alfvén speed of the solar wind was comparable to the solar wind flow speed. As a result, the proton energy gained through Alfvénic reconnection bulk acceleration was ~3 times that of the surrounding solar wind core energy, making the exhaust proton population clearly distinguishable from the ambient solar wind core protons.

For the E08 HCS, this has allowed the clear identification of protons leaking out of the local reconnecting HCS along separatrix field lines. The leaked protons appeared as energetic proton beams (with energies up to at least 2.5 keV, and possibly up to 40 keV/nucleon) clearly separated from the core solar wind when detected far from the HCS (Figure 2e). Similar distributions have been reported by Verniero et al. (2020), although it is not clear how far away from the HCS those observations were. The interpretation of leaked proton beams is supported by the concurrent dropouts of superthermal strahl electrons, consistent with the spacecraft sampling the separatrix layer of an anti-sunward exhaust that is magnetically disconnected from the Sun.

For E07, energetic proton beams were also observed in broad regions surrounding both sides of the HCS. However, in contrast to E08, there were no clear dropouts of superthermal (e.g., 314 eV) field-aligned electrons associated with the presence of most proton beams. The lack of 314eV electron dropouts could mean the absence of separatrix layers (i.e., the exhaust boundaries were tangential discontinuities), and that the source of proton beams was not the HCS exhaust. However, in Section 4.3, we pointed out the possibility of a remote source for both the proton beams and the field-aligned superthermal electrons. A challenge to justify any source sunward of the reconnection X-line in this event is to understand how such particles can penetrate into the region close to the reconnection exhaust with no discernable gap associated with separatrix field lines. Separatrix signatures might, of course, be more complex when reconnection is intermittent or patchy (in 3D), or when the HCS contains multiple active and non-active X-lines/flux ropes (e.g., Gosling et al., 1995; Khabarova et al., 2015; Shepherd et al., 2017; Sanchez-Diaz et al., 2019; Lavraud et al., 2020; Réville et al., 2020).

In conclusion, PSP observations have shown that reconnection in the near-Sun HCS produces high-energy protons seen in a broad region outside the HCS. The leaked proton beam energy is simply related to the energy of the accelerated protons inside the exhaust, which in turns depends on the available magnetic energy per particle in the local solar wind. Thus, reconnection in the near-Sun HCS produces beams at much higher energies than at 1 AU. Further PSP observations closer to the Sun will shed more light on the relationship between reconnection and accelerated proton beams in the solar wind.

Acknowledgments

We are grateful for the dedicated efforts of the entire Parker Solar Probe team. We acknowledge NASA FIELDS contract NNN06AA01C and NASA SWEAP contract NNN06AA01C. Data source: http://fields.ssl.berkeley.edu/data/ and http://sweap.cfa.harvard.edu/pub/data/sci/sweap/.

References

Akhavan-Tafti, M., J Kasper, J Huang, S Bale (2021), Discontinuity analysis of the leading switchback transition regions, *A&A*, 650, https://doi.org/10.1051/0004-6361/202039508.

Bale, S. D., Goetz, K., Harvey, P. R., et al. (2016), The FIELDS Instrument Suite for Solar Probe Plus, *Space Science Rev.*, 204, 49, doi: 10.1007/s11214-016-0244-5

Cassak, P. A., and M. A. Shay (2007), Scaling of asymmetric magnetic reconnection: General theory and collisional simulations, *Physics of Plasmas*, 14, 102114.

Davis, M.S., Phan, T.D., Gosling, J.T., Skoug, R.M. (2006), Detection of oppositely directed reconnection jets in a solar wind current sheet, *Geophys. Res. Lett.*, 33, L19102.

Desai, M. I., et al. (2021), Suprathermal Ion Energy spectra and Anisotropies near the Heliospheric Current Sheet crossing observed by the Parker Solar Probe during Encounter 7, *ApJ*, http://arxiv.org/abs/2111.00954.

Drake, J. F., et al. (2009), Ion heating resulting from pickup in magnetic reconnection exhausts, *J. Geophys. Res.*, 114, 5111, doi:10.1029/2008JA013701.

Eastwood, J. P., R. Mistry, T. D. Phan, S. J. Schwartz, R. E. Ergun, J. F. Drake, et al., Guide field reconnection: Exhaust structure and heating, *Geophys. Res. Lett.*, 45, https://doi.org/10.1029/2018GL077670, 2018.

Eastwood, J. P., J. E. Stawarz, T. D. Phan, et al. (2021), Solar Orbiter observations of an ion-scale flux rope confined to a bifurcated solar wind current sheet, *A&A*, doi:https://doi.org/10.1051/0004-6361/202140949

Eriksson, S., Gosling, J. T., Phan, T. D., et al. (2009), Asymmetric shear flow effects on magnetic field configuration within oppositely directed solar wind reconnection exhausts. *J. Geophys. Res.*, 114, A07103.

Froment, C., V., K., Dudok de Wit, T., et al. (2021), Direct evidence for magnetic reconnection at the boundaries, *A&A*, 650, A5, https://doi.org/10.1051/0004-6361/202039806.

Gosling, J. T., J. Birn, and M. Hesse (1995), Three-dimensional magnetic reconnection and the magnetic topology of coronal mass ejection events, *Geophys. Res. Lett*., 22, 8.

Gosling, J. T., R. M. Skoug, D. J. McComas, and C. W. Smith (2005a), Direct evidence for magnetic reconnection in the solar wind near 1 AU, *J. Geophys. Res.,* 110, A01107, doi:10.1029/2004JA010809.

Gosling, J. T., Skoug, R. M., McComas, D. J., & Smith, C. W. (2005b), Magnetic reconnection at the heliospheric current sheet and the formation of closed magnetic field lines in the solar wind, *Geophys. Res. Lett*., 32, L05105.

Gosling, J. T., et al., 2006, Magnetic reconnection at the heliospheric current sheet and the formation of closed magnetic field lines in the solar wind, *Geophys. Res. Lett*., 33, 17, https://doi.org/10.1029/2006GL027188.

Gosling, J. T., T. D. Phan, R. P. Lin, and A. Szabo (2007), Prevalence of magnetic reconnection at small field shear angles in the solar wind, *Geophys. Res. Lett*., 34, L15110, doi:10.1029/2007GL030706.

Gosling, J. T. and T. D. Phan (2013), Magnetic reconnection in the solar wind at current sheets associated with extremely small field shear angles, *ApJ.* L39 doi: 10.1088/2041-8205/763/2/L39.

Haggerty, C. C., et al. (2015), The competition of electron and ion heating during magnetic reconnection, *Geophys. Res. Lett*., 42, 22, https://doi.org/10.1002/2015GL065961.

Halekas, J. S., Whittlesey, P., Larson, D. E., et al. (2020), Electrons in the Young Solar Wind: First Results from the Parker Solar Probe, *ApJS*, 246, 22.

Huttunen, K.E.J., Bale, S.D., Salem, C. (2008), Wind observations of low energy particles within a solar wind reconnection region, *Ann. Geophys*. 26, 2701, https://doi.org/10.5194/angeo-26-2701-2008.

Kasper, J. C., Abiad, R., Austin, G., et al. (2016), Solar Wind Electrons Alphas and Protons (SWEAP) Investigation: Design of the Solar Wind and Coronal Plasma Instrument Suite for Solar Probe Plus, *Space Science Rev*., 204, 131, doi: 10.1007/s11214-015-0206-3

Khabarova, O., G. Zank, G. Li., et al. (2015), Small-scale magnetic islands in the solar wind and their role in particle acceleration. I. Dynamics of magnetic islands near the heliospheric current sheet, *ApJ*, 808, 181, http://dx.doi.org/10.1088/0004-637X/808/2/181.

Khabarova, O. V. and Zank, G. P. 2017, Energetic Particles of keV–MeV Energies Observed near Reconnecting Current Sheets at 1 au, *ApJ*, 843, 1, doi:10.3847/1538-4357/aa7686.

Lavraud, B., et al. (2002), Cluster observations of the exterior cusp and its surrounding boundaries under northward IMF, Geophys. Res. Lett., 29, 20, doi:10.1029/2002GL015464.

Lavraud, B., Gosling, J. T., Rouillard, A. P., et al. (2009), Observation of a Complex Solar Wind Reconnection Exhaust from Spacecraft Separated by over 1800 R_E, *SoPh*, 256, 379

Lavraud, B. A., Ruffenach, A., Rouilldard, A., et al. (2014), Geo-effectiveness and radial dependence of magnetic cloud erosion by magnetic reconnection, *J. Geophys. Res*., 119, doi:10.1002/2013JA019154

Lavraud, B., et al. 2021, Magnetic reconnection as a mechanism to produce multiple proton populations and beams locally in the solar wind, *A&A*, doi: https://doi.org/10.1051/0004-6361/202141149.

Livi. R., Larson, D. E., Kasper, J. C., et al. (2020), The Solar Probe ANalyzer -Ions on Parker Solar Probe, ApJS, doi: doi.org/10.1002/essoar.10508651.1.

McComas, D. J., Alexander, N., Angold, N., et al. (2016), Integrated Science Investigation of the Sun (ISIS): Design of the Energetic Particle Investigation, *Space Science Rev*., 204, 187, doi: 10.1007/s11214-014-0059-1

Mistry, R., Eastwood, J. P., Phan, T. D., & Hietala, H. (2015), Development of bifurcated current sheets in solar wind reconnection exhausts, *Geophys. Res. Lett*., 42, 24, https://doi.org/10.1002/2015GL066820.

Mistry, R., Eastwood, J. P., Phan, T. D., & Hietala, H. (2017), Statistical properties of solar wind reconnection exhausts, *J. Geophys. Res*., 122, 6, https://doi.org/10.1002/2017JA024032.

Onsager, T. G., M . F. Thomsen, R. C. Elphic, and J. T. Gosling (1991), Model of electron and ion distributions in the plasma sheet boundary layer, *J. Geophys. Res., 96*, A12.

Petschek, H. E., (1964), Magnetic Field Annihilation, Proceedings of the AAS-NASA Symposium, Edited by Wilmot N. Hess. Washington, DC: National Aeronautics and Space Administration, Science and Technical Information Division, 425.

Phan, T. D., Gosling, J. T., Davis, M. S., et al. (2006), A magnetic reconnection X-line extending more than 390 Earth radii in the solar wind, *Nature*, 439, 175.

Phan, T. D., et al. (2007), Evidence for magnetic reconnection initiated in the magnetosheath, *Geophys. Res. Lett.*, 34, 14, https://doi.org/10.1029/2007GL030343.

Phan, T. D., et al. (2010), The dependence of magnetic reconnection on plasma β and magnetic shear: Evidence from solar wind observations, *ApJ., 719,* doi:10.1088/2041-8205/719/L199.

Phan, T. D., et al. (2013), Electron bulk heating in magnetic reconnection at Earth's magnetopause: Dependence on inflow Alfvén speed and magnetic shear, *Geophys. Res. Lett.,* 40, doi:10.1002/grl.50917.

Phan, T. D., Drake, J. F., Shay, et al. (2014), Ion bulk heating in magnetic reconnection exhausts at Earth's magnetopause: Dependence on the inflow Alfvén speed and magnetic shear angle, *Geophys. Res. Lett*., 41, 20, https://doi.org/10.1002/2014GL061547.

Phan, T. D., Bale, S. D., Eastwood, J. P., et al. (2020), Parker Solar Probe In Situ Observations of Magnetic Reconnection Exhausts during Encounter 1, *ApJS*, 246, 34.

Phan, T. D., et al. 2021, Prevalence of Magnetic Reconnection in the near-Sun Heliospheric Current Sheet, *A&A*, 650, A13, https://doi.org/10.1051/0004-6361/202039863

Pulupa, M. P., et al. (2014), Core electron heating in solar wind reconnection exhausts, *ApJL*, 791(1):L17, doi:10.1088/2041-8205/791/1/L17.

Réville, V., Velli, M., A. P. Rouillard, et al. (2020), Tearing Instability and Periodic Density Perturbations in the Slow Solar Wind, *ApJL*, 895, 1, doi:10.3847/2041-8213/ab911d.

Ruffenach, A., et al. (2012), Multispacecraft observation of magnetic cloud erosion by magnetic reconnection during propagation, *J. Geophys. Res*., 117, A09101, https://doi.org/10.1029/2012JA017624.

Ruffenach, A., et al. (2015), Statistical study of magnetic cloud erosion by magnetic reconnection, *J. Geophys. Res*., 120, doi:10.1002/2014JA020628, 2015.

Shepherd, L. S., P. A. Cassak, J. F. Drake, J. T. Gosling, T. D. Phan, M. A, Shay (2017), Structure of Exhausts in Magnetic Reconnection with an X-line of Finite Extent, *ApJ*, 848, 2, doi: 10.3847/1538-4357/aa9066.

Sonnerup, B. U. Ö., and L. J. Cahill Jr. (1967), Magnetopause structure and attitude from Explorer 12 observations, *J. Geophys. Res., 72,* 171.

Swisdak, M., et al. (2003), Diamagnetic suppression of component magnetic reconnection at the magnetopause, *J. Geophys. Res*., *108,* 1218.

Swisdak, M., et al. (2010), The vector direction of the interstellar magnetic field outside the heliosphere, *ApJ, 710,* doi:10.1088/0004-637X/710/1769.

Szabo, A., Larson, D. E., Whittlesey, P., et al. (2020), The Heliospheric Current Sheet in the Inner Heliosphere Observed by the Parker Solar Probe, *ApJS*, 246, 47, doi:10.3847/1538-4365/ab5dac.

Whittlesey, P. L., Larson, D. E., Kasper, J. C, et al. (2020), The Solar Probe ANalyzers—Electrons on the Parker Solar Probe, *ApJS*, 246, 74.

Figure Captions

Figure 1. PSP crossing of a reconnecting HCS near E08 perihelion, displaying large plasma acceleration in the exhaust and energetic proton beams outside the HCS. (a) Ion spectrogram from ISOIS/EPI-Lo, in counts/energy bin, (b,c) proton and electron spectrograms in differential energy flux ($eVs^{-1}cm^{-2}ster^{-1}eV^{-1}$), (d) pitch angle distribution of 314eV electrons, (e,f) magnitude and components of the magnetic field in RTN, (g-h) proton velocity and density, (i-j) proton and electron temperatures, (k) schematic illustration of the standard reconnection exhaust and separatrix layers and the RTN coordinates. The slanted (black) field lines in the exhaust is due to

Alfvén waves propagating at higher speed on the upper side. The vertical dashed lines mark the edges of the exhaust. The proton moments are in the Sun's frame. The nearly indistinguishable black and green curves in panel (c) are twice the core electron temperature and the peak in differential energy fluxes.

Figure 2. Proton distributions inside in the exhaust and in the adjacent separatrix layer of the same HCS as in Figure 1. (a) Magnetic field in RTN, (b-d) proton radial velocity, temperatures, and spectrograms, (e-h) proton distributions summed and collapsed onto θ-plane in SPAN-I instrument coordinates (see Verniero et al., 2020): (e) near the outer edge of separatrix layer, (f) in the separatrix layer closer to the HCS, (g) in the exhaust near the left edge, (h) in the weak |**B**| region of the exhaust, and (i) schematics of the reconnection exhaust and separatrix layers, and the locations where the protons distributions e-h were sampled. The yellow arrow in panels e-h points along **B**, and its length represents the local Alfvén speed.

Figure 3. PSP crossing of a reconnecting HCS near E07 perihelion. The parameters are the same as in Figure 1.

Figure 4. Zoom-out of Figure 3 showing broad regions surrounding the PSP crossing of the E07 HCS. The parameters are the same as in Figure 1. The black dashed lines mark the two edges of the complete crossing of the HCS. The interval between the two green dashed lines is a partial HCS crossing. The left and right blue dashed lines mark the outer boundaries of the regions surrounding the HCS that showed persistent $T_{p\|}>T_{p\perp}$.

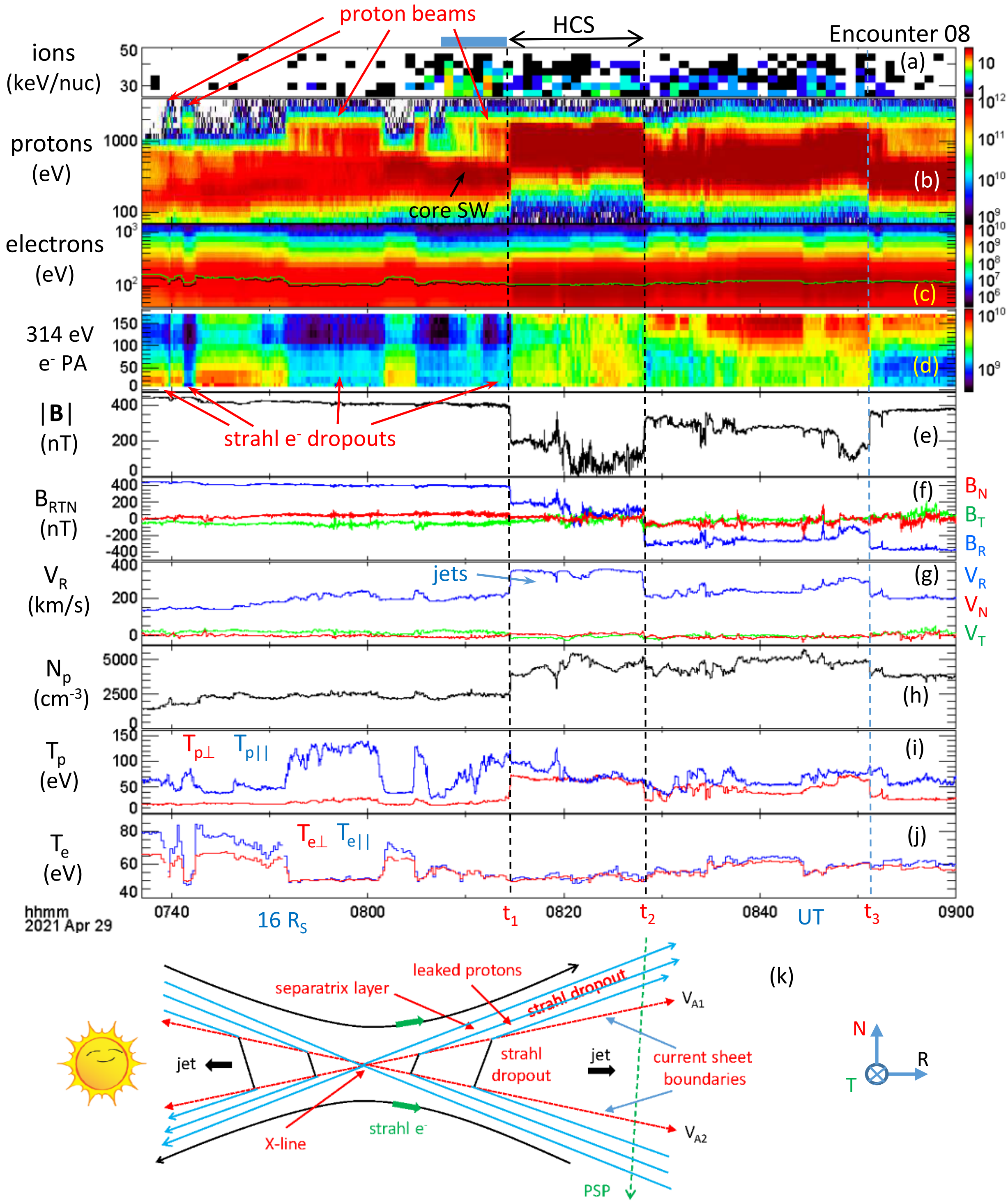

Figure 1. PSP crossing of a reconnecting HCS near E08 perihelion, displaying large plasma acceleration in the exhaust and energetic proton beams outside the HCS. (a) Ion spectrogram from ISOIS/EPI-Lo, in counts/energy bin, (b,c) proton and electron spectrograms in differential energy flux ($eVs^{-1}cm^{-2}ster^{-1}eV^{-1}$), (d) pitch angle distribution of 314eV electrons, (e,f) magnitude and components of the magnetic field in RTN, (g-h) proton velocity and density, (i-j) proton and electron temperatures, (k) schematic illustration of the standard reconnection exhaust and separatrix layers and the RTN coordinates. The slanted (black) field lines in the exhaust is due to Alfvén waves propagating at higher speed on the upper side. The vertical dashed lines mark the edges of the exhaust. The proton moments are in the Sun's frame. The nearly indistinguishable black and green curves in panel (c) are twice the core electron temperature and the peak in differential energy fluxes.

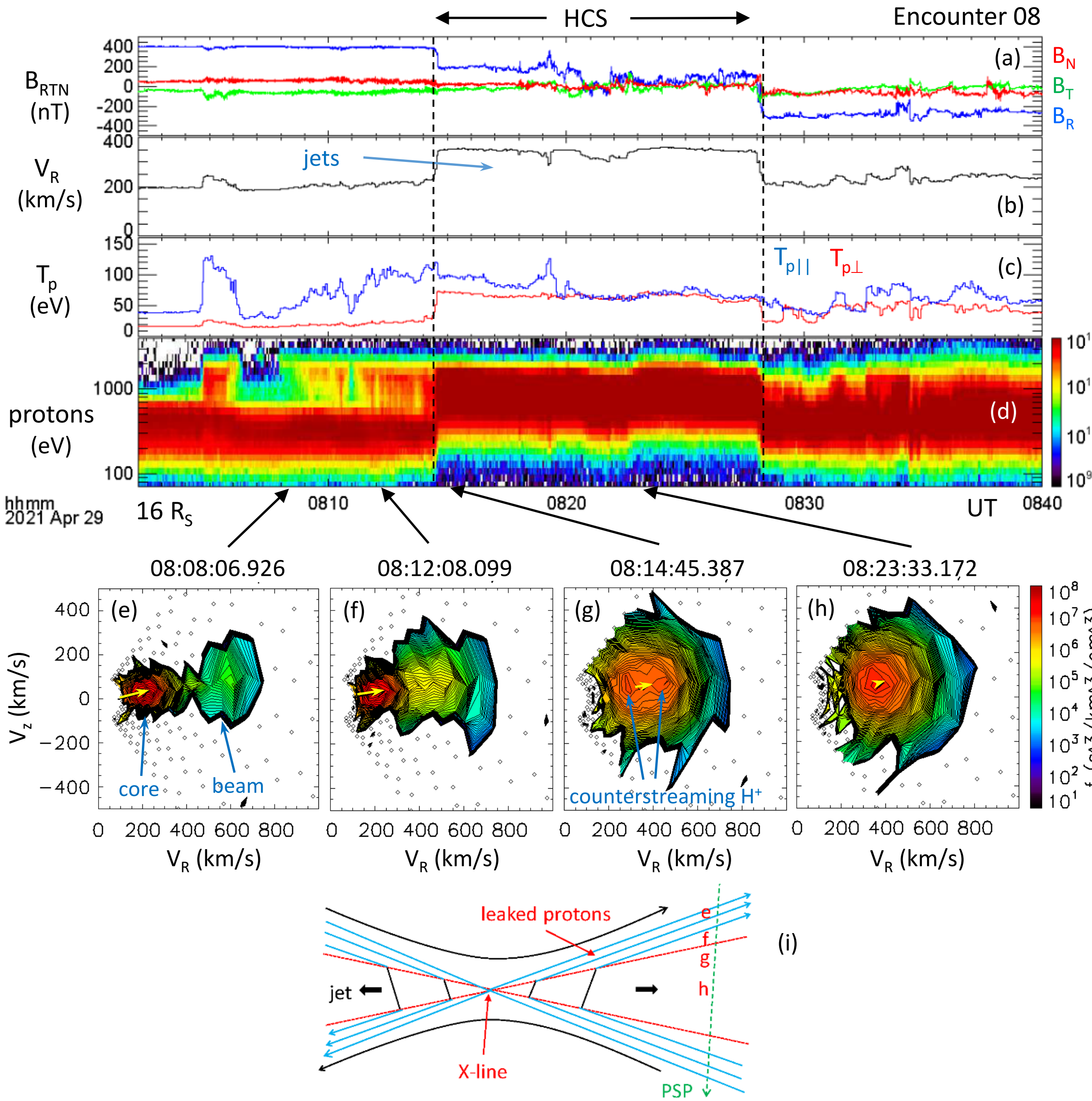

Figure 2. Proton distributions inside in the exhaust and in the adjacent separatrix layer of the same HCS as in Figure 1. (a) Magnetic field in RTN, (b-d) proton radial velocity, temperatures, and spectrograms, (e-h) proton distributions summed and collapsed onto θ-plane in SPAN-I instrument coordinates (see Verniero et al., 2020): (e) near the outer edge of separatrix layer, (f) in the separatrix layer closer to the HCS, (g) in the exhaust near the left edge, (h) in the weak |**B**| region of the exhaust, and (i) schematics of the reconnection exhaust and separatrix layers, and the locations where the protons distributions e-h were sampled. The yellow arrow in panels e-h points along **B**, and its length represents the local Alfvén speed.

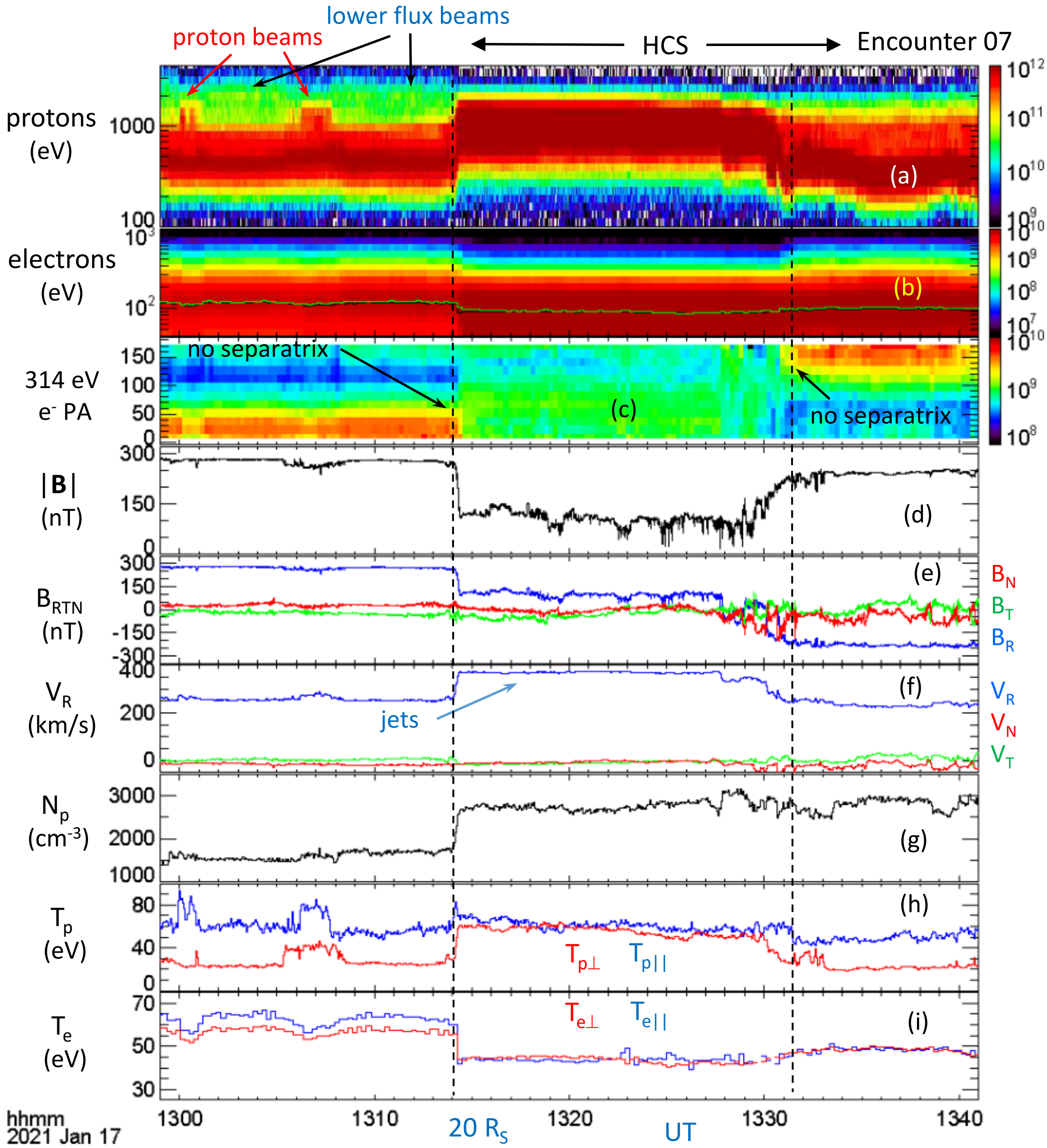

Figure 3. PSP crossing of a reconnecting HCS near E7 perihelion. The parameters are the same as in Figure 1.

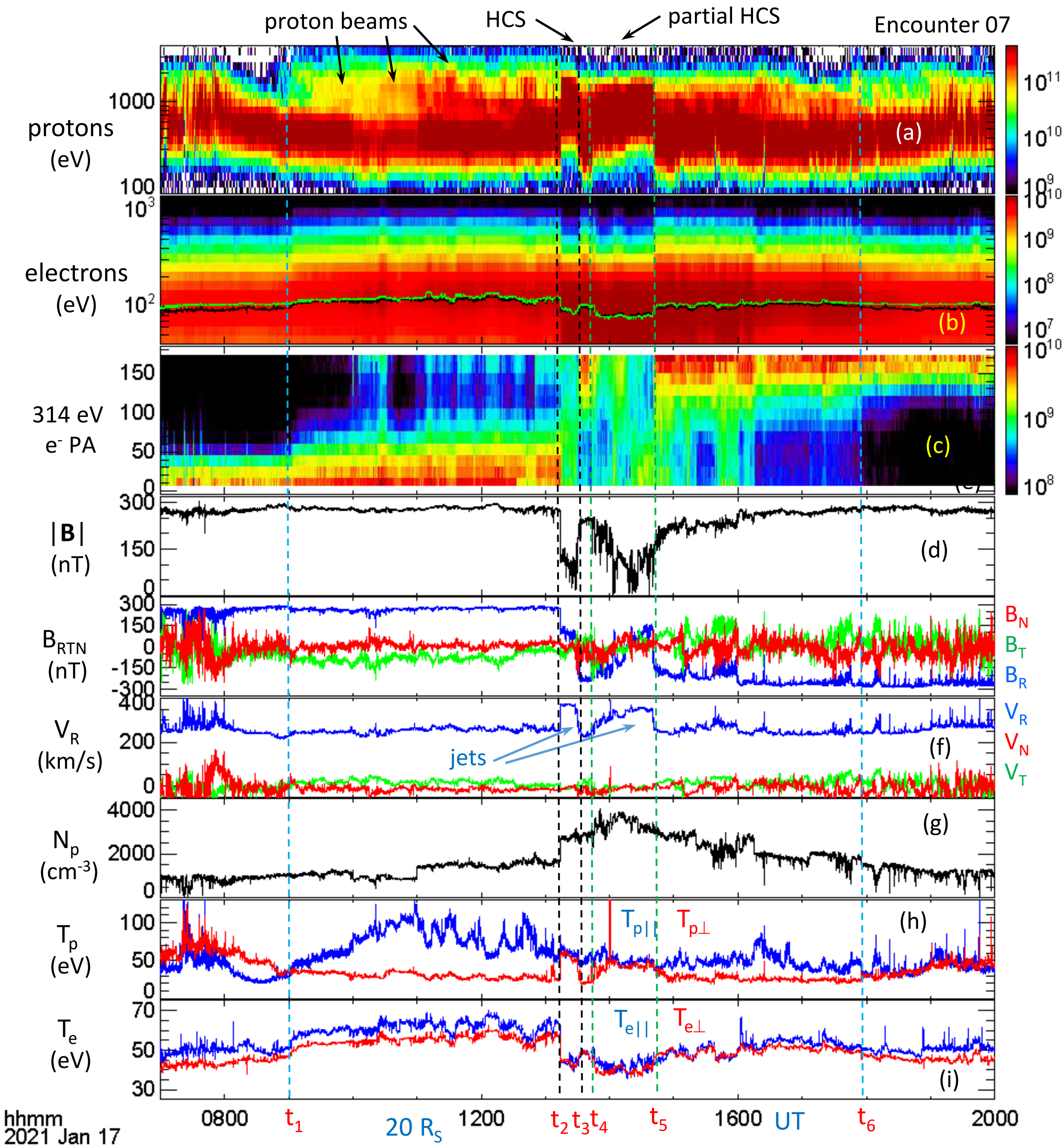

Figure 4. Zoom-out of Figure 3 showing broad regions surrounding the PSP crossing of the E07 HCS. The parameters are the same as in Figure 1. The black dashed lines mark the two edges of the complete crossing of the HCS. The interval between the two green dashed lines is a partial HCS crossing. The left and right blue dashed lines mark the outer boundaries of the regions surrounding the HCS that showed persistent $T_{p\|}>T_{p\perp}$.